

LETTERS

Loss of autophagy in the central nervous system causes neurodegeneration in mice

Masaaki Komatsu^{1,2*}, Satoshi Waguri^{3*†}, Tomoki Chiba¹, Shigeo Murata¹, Jun-ichi Iwata^{1,2}, Isei Tanida², Takashi Ueno², Masato Koike³, Yasuo Uchiyama³, Eiki Kominami² & Keiji Tanaka¹

Protein quality-control, especially the removal of proteins with aberrant structures, has an important role in maintaining the homeostasis of non-dividing neural cells¹. In addition to the ubiquitin–proteasome system, emerging evidence points to the importance of autophagy—the bulk protein degradation pathway involved in starvation-induced and constitutive protein turnover—in the protein quality-control process^{2,3}. However, little is known about the precise roles of autophagy in neurons. Here we report that loss of *Atg7* (autophagy-related 7), a gene essential for autophagy, leads to neurodegeneration. We found that mice lacking *Atg7* specifically in the central nervous system showed behavioural defects, including abnormal limb-clasping reflexes and a reduction in coordinated movement, and died within 28 weeks of birth. *Atg7* deficiency caused massive neuronal loss in the cerebral and cerebellar cortices. Notably, polyubiquitinated proteins accumulated in autophagy-deficient neurons as inclusion bodies, which increased in size and number with ageing. There was, however, no obvious alteration in proteasome function. Our results indicate that autophagy is essential for the survival of neural cells, and that impairment of autophagy is implicated in the pathogenesis of neurodegenerative disorders involving ubiquitin-containing inclusion bodies.

Macroautophagy (hereafter referred to as autophagy) is an evolutionarily conserved pathway in which the cytoplasm and organelles are engulfed within double-membraned vesicles, known as autophagosomes, in preparation for the turnover and recycling of these cellular constituents⁴. Genetic studies using various model organisms have highlighted the importance of autophagy in physiological and pathological events⁵. The principal role of autophagy is in the supply of nutrients for survival, as shown in yeast⁶ and early neonatal mice^{7,8}. Autophagy also has a role in cellular remodelling during differentiation and the development of multicellular organisms, such as dauer formation in *Caenorhabditis elegans*⁹ and metamorphosis in *Drosophila melanogaster*¹⁰. Moreover, constitutive autophagy, which occurs independently of nutrient stress, contributes to mouse liver homeostasis⁸, major histocompatibility class (MHC) II antigen presentation¹¹, and cellular defence against invading streptococci¹² and *Mycobacterium tuberculosis*¹³. However, the physiological functions of autophagy, particularly in neurons, are still largely unknown.

To examine the relationship between neuronal pathology and autophagy deficiency *in vivo*, we crossed *Atg7*-conditional knockout mice (*Atg7^{flox/flox}*) (ref. 8) with transgenic mice expressing Cre recombinase under the control of the nestin promoter (*nestin-Cre*) (ref. 14), to produce mice deficient for *Atg7* specifically in the central nervous system (*Atg7^{flox/flox}; nestin-Cre*). *Atg7* is an E1-like enzyme for both the Atg12- and Atg8-conjugation systems¹⁵, and is essential

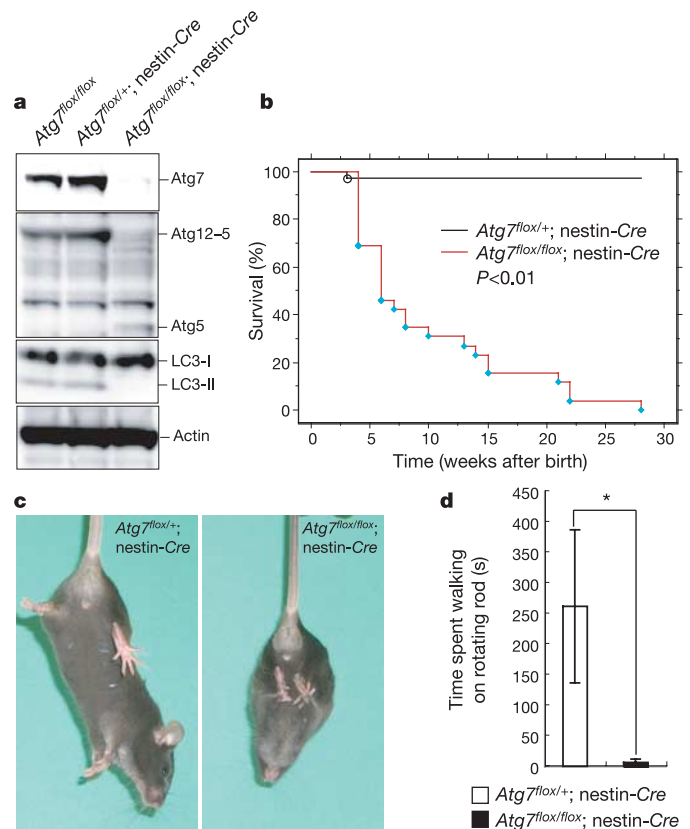


Figure 1 | Behavioural disorder in *Atg7^{flox/flox}; nestin-Cre* mice.

a, Impairment of two ATG-conjugation systems (Atg12 and LC3) in the *Atg7*-deficient brain. Brain homogenates from P28 mice were immunoblotted with antibodies against Atg7, Atg5 and LC3. Actin was used as a loading control. Data shown are representative of three separate experiments. **b**, Kaplan–Meier survival curves of *Atg7^{flox/+}; nestin-Cre* ($n = 41$) and *Atg7^{flox/flox}; nestin-Cre* ($n = 26$) mice over 28 weeks. **c**, Abnormal limb-clasping reflexes in *Atg7^{flox/flox}; nestin-Cre* mice at P28. When lifted by the tail, *Atg7^{flox/+}; nestin-Cre* mice behave normally, extending their hind limbs and bodies. In contrast, *Atg7^{flox/flox}; nestin-Cre* mice bend their legs towards their trunk or tighten their back limbs to their bodies and anterior limbs. **d**, Movement ataxia in *Atg7^{flox/flox}; nestin-Cre* mice at P28. Motor coordination was tested using a rotarod assay. *Atg7^{flox/+}; nestin-Cre* ($n = 5$) and *Atg7^{flox/flox}; nestin-Cre* ($n = 5$) mice were placed on a rod rotating at 20 r.p.m., and the time spent on the rod was counted. Data show mean \pm s.d. *, $P < 0.01$ (Student's *t*-test). There was no significant sex difference in survival rate and onset-stage of abnormal limb-clasping and tremor in *Atg7^{flox/flox}; nestin-Cre* mice.

¹Laboratory of Frontier Science, Tokyo Metropolitan Institute of Medical Science, Bunkyo-ku, Tokyo 113-8613, Japan. ²Department of Biochemistry, Juntendo University School of Medicine, Bunkyo-ku, Tokyo 113-8421, Japan. ³Department of Cell Biology and Neurosciences, Osaka University Graduate School of Medicine, Osaka 565-0871, Japan. [†]Present address: Department of Anatomy and Histology, Fukushima Medical University School of Medicine, 1 Hikarigaoka, Fukushima 960-1295, Japan.

*These authors contributed equally to this work.

for autophagy⁸. Atg7 protein was absent at postnatal day (P)28 in brain from *Atg7^{fllox/fllox}; nestin-Cre* but not control (*Atg7^{fllox/+}; nestin-Cre*) mice (Fig. 1a). The level of Atg7 protein in other tissues such as liver, lung, heart and muscle was comparable between *Atg7^{fllox/fllox}; nestin-Cre* and control mice (data not shown). Atg12–Atg5 conjugate was detected only in the brains of control mice by immunoblotting with an anti-Atg5 antibody (Fig. 1a). In contrast, free Atg5, which was faintly observed in the control mouse brain, was clearly increased in the mutant brain (Fig. 1a). The mammalian homologue of yeast Atg8, microtubule-associated protein 1 light-chain 3 (LC3), exists in two forms (LC3-I and LC3-II)¹⁶. Both forms were detected in brains from control mice, but only the LC3-I form was detected in *Atg7^{fllox/fllox}; nestin-Cre* brain (Fig. 1a). The loss of both Atg7 and LC3-II proteins was observed from P0 in the brain of *Atg7^{fllox/fllox}; nestin-Cre* mice (Supplementary Fig. S1). These results indicate complete impairment of autophagy in the central nervous system of *Atg7^{fllox/fllox}; nestin-Cre* mice after birth.

Atg7^{fllox/fllox}; nestin-Cre mice were viable at birth and indistinguishable in appearance from their littermates. However, the survival rate of the mutant mice diminished markedly by four weeks after birth, and all *Atg7^{fllox/fllox}; nestin-Cre* mice were dead within 28 weeks

(Fig. 1b). We also observed growth retardation as early as P14 in these mice (data not shown). Furthermore, the mice showed motor and behavioural deficits, including abnormal limb-clasping reflexes (Fig. 1c) and tremor, and in some cases, they walked on their tiptoes. In a rotarod test, most *Atg7^{fllox/fllox}; nestin-Cre* mice fell after grasping the rod only briefly (Fig. 1d). These motor and behavioural deficits began to appear at P14–P21. These results suggest that autophagy deficiency in the central nervous system results in a severe neurological disorder.

Histological analysis using Meyer's haematoxylin and eosin (H&E) staining showed marked atrophy of the cerebral cortical region of *Atg7^{fllox/fllox}; nestin-Cre* brain at P56 (Fig. 2a, b). The ratios of cortical thickness to dorsoventral thickness of the brain in *Atg7^{fllox/+}; nestin-Cre* and *Atg7^{fllox/fllox}; nestin-Cre* mice were 0.17 ± 0.00031 and 0.15 ± 0.00034 , respectively ($n = 5$, $P < 0.01$). Notably, almost no large pyramidal neurons were observed in *Atg7^{fllox/fllox}; nestin-Cre* mice compared with the corresponding region in brains from control mice (Fig. 2c, d). Immunostaining for the glial marker GFAP (glial fibrillary acidic protein) showed an increase in GFAP signal in the cerebral cortex of *Atg7^{fllox/fllox}; nestin-Cre* mice (Fig. 2e, f), suggesting the presence of neuronal damage in this region. In the cerebellar

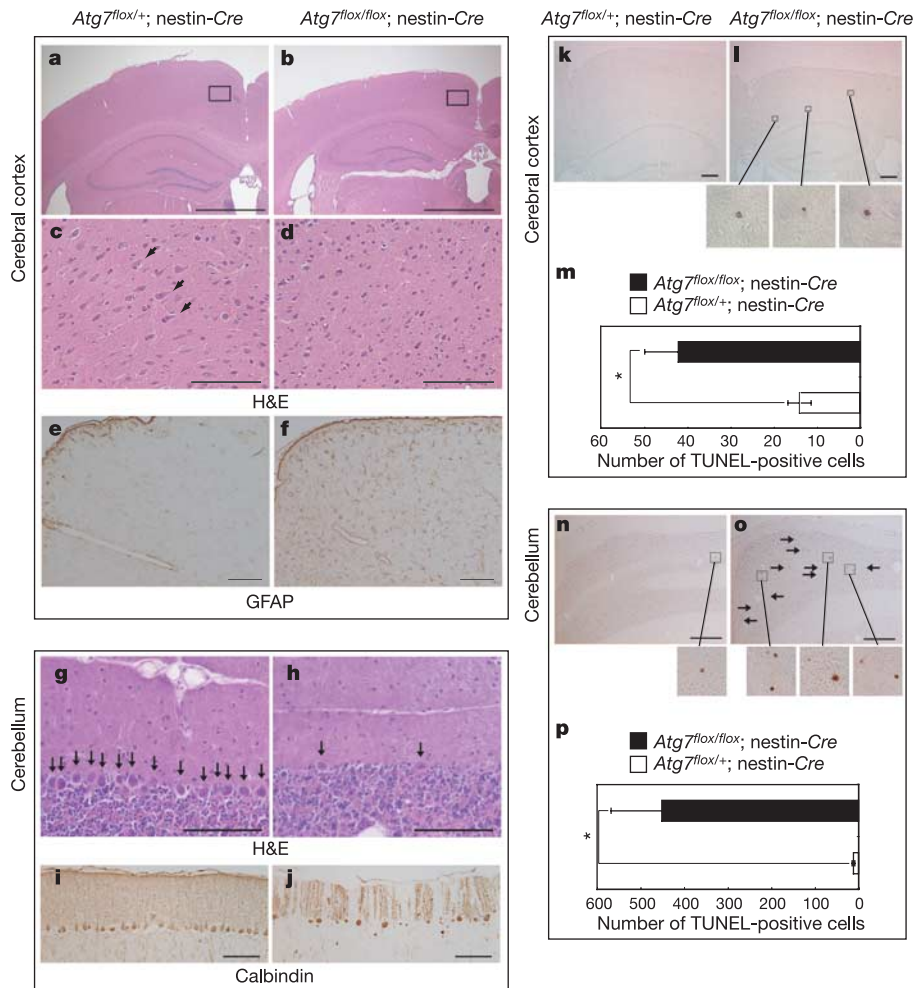


Figure 2 | Marked cell death in autophagy-deficient cerebral cortex and cerebellum. **a–f**, Histological analyses of *Atg7^{fllox/+}; nestin-Cre* (left) and *Atg7^{fllox/fllox}; nestin-Cre* (right) cerebral cortex at P56. Cryosections were stained with H&E (**a–d**) or immunostained for the glial marker GFAP (**e, f**). Boxed areas in **a** and **b** are magnified in **c** and **d**, respectively. Arrows in **c** point to large pyramidal neurons in the cerebral cortex. **g–j**, Histological analysis of *Atg7^{fllox/+}; nestin-Cre* (left) and *Atg7^{fllox/fllox}; nestin-Cre* (right) cerebellum at P56. Cryosections were stained with H&E (**g, h**) or immunostained for the Purkinje marker calbindin (**i, j**). Arrows in **g** and **h**

indicate cerebellar Purkinje cells. **k–p**, TUNEL staining of the cerebral cortex (**k, l**) and cerebellum (**n, o**) at P56 in *Atg7^{fllox/+}; nestin-Cre* (**k, n**) and *Atg7^{fllox/fllox}; nestin-Cre* (**l, o**) sections. TUNEL-positive cells are indicated with arrows and shown as higher magnification images beneath panels **l, n** and **o**. Histograms show the average number (\pm s.d.) of TUNEL-positive cells in ten sections for three animals of each genotype (**m, p**). *, $P < 0.05$ (t -test). Scale bars, 1 mm (**a, b**), 100 μ m (**c–j**), 250 μ m (**k, l, n, o**). We observed no sex difference in brain morphology or neuronal loss in *Atg7^{fllox/fllox}; nestin-Cre* mice.

cortex, H&E staining revealed a large reduction in the number of Purkinje cells in the mutant brain (Fig. 2g, h), which was further confirmed by immunolabelling of Purkinje cells with an anti-calbindin antibody (Fig. 2i, j). Similar neuronal loss was also recognized in the hippocampal pyramidal cell layer of mutant brain (Supplementary Fig. S2).

To determine whether the reduced number of neurons observed in *Atg7^{flox/flox}; nestin-Cre* mouse brain was caused by cell death, we performed TUNEL (TdT-mediated dUTP nick end labelling) assays. We observed a marked increase in the number of TUNEL-positive cells in the cerebral cortex (Fig. 2k–m) and granular cell layer of the cerebellum at P56 in *Atg7^{flox/flox}; nestin-Cre* mice (Fig. 2n–p) compared with control mouse brains. Although loss of Purkinje cells was observed in the mutant brain, we could not detect TUNEL-positive Purkinje cells at any developmental stage examined. However, when *Atg7* was specifically depleted in Purkinje cells using transgenic mice expressing Cre recombinase under the control of the *Pcp2* gene

promoter (*Pcp2-Cre*), a marked reduction in the number of Purkinje cells was detected in the absence of TUNEL reactivity (data not shown), suggesting that neurons deficient in autophagy can die in a cell-autonomous fashion. Together, these results indicate that lack of autophagy in the central nervous system leads to neurodegeneration.

We have previously reported that autophagy is responsible for constitutive protein turnover in quiescent hepatocytes even under nutrient-rich conditions, and that a defect in autophagy leads to the accumulation of large, ubiquitin-containing inclusion bodies⁸. We therefore probed brain sections with an anti-ubiquitin antibody to examine the presence of ubiquitin-containing inclusion bodies. At P56, ubiquitin-positive dots were detected in several regions of the *Atg7^{flox/flox}; nestin-Cre* mouse brain, including the cerebral cortex (Fig. 3b), cerebellar Purkinje cells (Fig. 3d), hippocampal pyramidal neurons (Fig. 3f), thalamus (data not shown), hypothalamus (Fig. 3h), amygdala (Fig. 3j) and pontine nuclei (Fig. 3l). The degree of staining varied by region. For example, whereas most neuronal

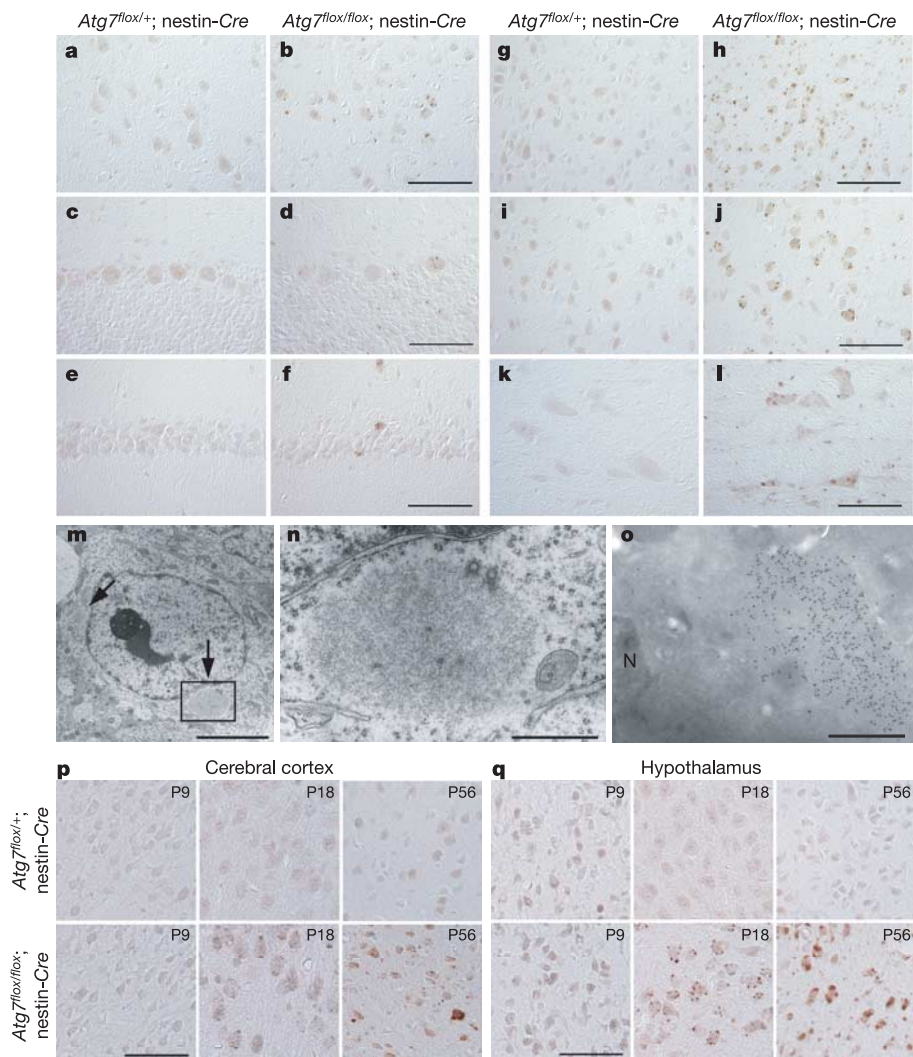


Figure 3 | Appearance of ubiquitin-positive inclusions in autophagy-deficient neurons. **a–l**, The presence of ubiquitin-positive dots was examined immunohistochemically in several regions including cerebral cortex (**a, b**), cerebellum (**c, d**), hippocampus (**e, f**), hypothalamus (**g, h**), amygdala (**i, j**) and pontine nuclei (**k, l**) of *Atg7^{flox+/+}; nestin-Cre* and *Atg7^{flox/flox}; nestin-Cre* mice. Note the presence of numerous ubiquitin dots in the amygdala and hypothalamus of the representative mutants. Scale bars, 50 μ m. **m, n**, Electron micrographs of the brain of *Atg7^{flox/flox}; nestin-Cre* mice. Inclusion bodies (arrows) were often observed in *Atg7^{flox/flox}; nestin-Cre* hypothalamus. The boxed region in **m** is shown in **n**. Inclusion bodies

were not detected in *Atg7^{flox+/+}; nestin-Cre* brain (data not shown). Scale bars, 5 μ m (**m**), 1 μ m (**n**). **o**, Immunoelectron micrograph of ubiquitin in a representative *Atg7^{flox/flox}; nestin-Cre* hypothalamus. N, nucleus. Scale bar, 1 μ m. **p, q**, Immunohistochemical detection of ubiquitin-positive inclusions in the cerebral cortex (**p**) and hypothalamus (**q**) at P9, P18 and P56. Brain sections of each genotype at the indicated ages were immunostained with an anti-ubiquitin antibody. Ubiquitin-positive inclusions appeared at P18 and became larger with ageing in the brain of *Atg7^{flox/flox}; nestin-Cre* mice. Scale bars, 50 μ m.

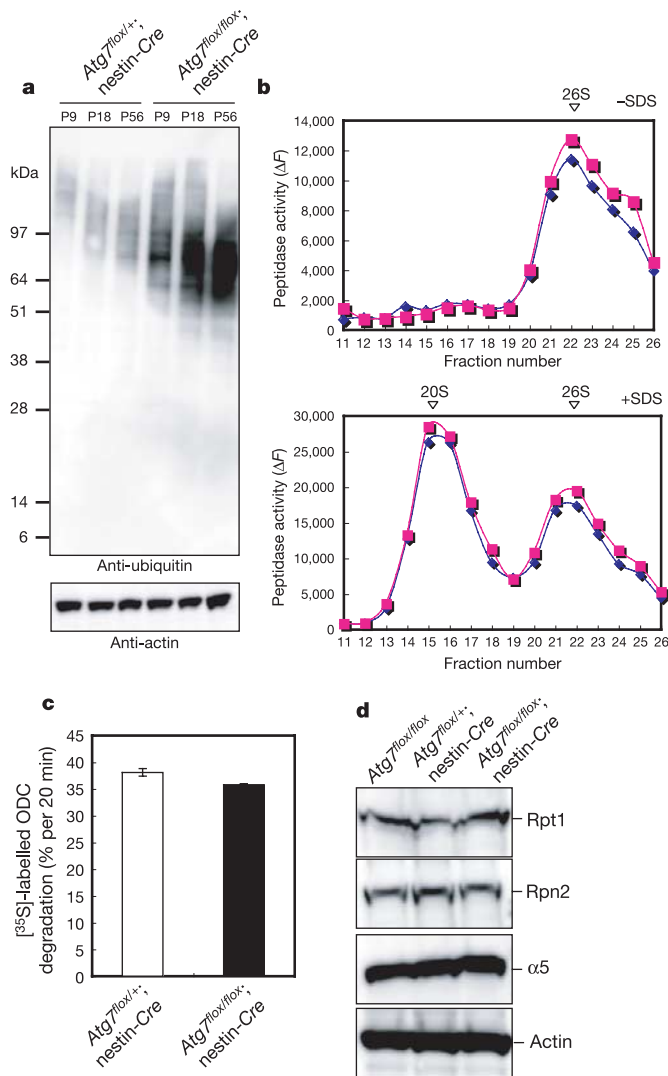


Figure 4 | Qualitative and quantitative analyses of proteasomes in autophagy-deficient brain. **a**, Increase in ubiquitinated proteins in *Atg7^{fllox/fllox}; nestin-Cre* mouse brain over time. Homogenates of P9, P18 and P56 brains from *Atg7^{fllox/fllox}; nestin-Cre* and *Atg7^{fllox/fllox}; nestin-Cre* mice were immunoblotted with an anti-ubiquitin antibody. An anti-actin antibody was used as a loading control. Data shown are representative of three separate experiments. We observed no sex difference in the accumulation of ubiquitin in *Atg7^{fllox/fllox}; nestin-Cre* mice. **b**, Peptide hydrolysis activity of 20S and 26S proteasomes. Homogenates from P28 *Atg7^{fllox/fllox}; nestin-Cre* (blue) and *Atg7^{fllox/fllox}; nestin-Cre* (pink) brains were fractionated by glycerol density gradient centrifugation (10–40% glycerol from fraction 1 to fraction 30). Aliquots from each fraction were used for the assay of chymotryptic activity of proteasomes using Suc-LLVY-AMC as a substrate in the absence (top) or presence (bottom) of 0.05% SDS. The sedimenting positions of 20S and 26S proteasomes are indicated with arrowheads. Note that whereas 26S proteasomes exist in active forms in tissues, 20S proteasomes are latent and are activated artificially by a low concentration of SDS. **c**, ATP-dependent degradation of [³⁵S]-labelled ODC. Degradation of [³⁵S]-labelled ODC was assayed using crude extracts from P28 *Atg7^{fllox/fllox}; nestin-Cre* and *Atg7^{fllox/fllox}; nestin-Cre* brains. The experiment was repeated three times, and values represent mean \pm s.d. In the above assays, there were no significant differences between *Atg7^{fllox/fllox}; nestin-Cre* and *Atg7^{fllox/fllox}; nestin-Cre* mice. **d**, Immunoblot analysis of 26S proteasome components. Homogenates from P28 *Atg7^{fllox/fllox}; nestin-Cre* and *Atg7^{fllox/fllox}; nestin-Cre* brains were immunoblotted with antibodies against the indicated proteins. Data shown are representative of three separate experiments. There was no change in proteasome status for the different genotypes.

cells in the amygdala (Fig. 3j) and hypothalamus (Fig. 3h) contained several ubiquitin dots of small to large size, only a small number of cerebellar Purkinje cells stained for ubiquitin, and the immunoreactive dots were of small size (Fig. 3d). Electron microscopy showed that *Atg7^{fllox/fllox}; nestin-Cre* hypothalamic neurons had circular or elliptical large structures composed of fibrillar elements in the perikarya (Fig. 3m, n). Immunoelectron microscopy further confirmed that these aberrant structures contained ubiquitin (Fig. 3o). These ubiquitin dots appeared not only in the perikarya of neurons, but also in the intercellular space (see Fig. 3h, j, l). Dots found in the intercellular space might correspond to ubiquitin inside neurites, because they were observed in myelinated axons around pontine nuclei using both light and electron microscopy (Supplementary Fig. S3a, b). In contrast, almost no ubiquitin dots were observed in astroglial cells (Supplementary Fig. S3c). Together with the results in Fig. 3, we concluded that most of the distinct ubiquitin dots were located in neurons.

We examined the development of ubiquitin-containing inclusion bodies at different stages by dissecting the brains of *Atg7^{fllox/+}; nestin-Cre* and *Atg7^{fllox/fllox}; nestin-Cre* mice at P9, P18 and P56. Only a few ubiquitin-positive aggregates were noted in the neurons of control and mutant cerebral cortex and hypothalamus at P9 (Fig. 3p, q). In contrast, several ubiquitin-containing inclusions were clearly noted in *Atg7^{fllox/fllox}; nestin-Cre* cortex and hypothalamus at P18, increasing in number and size by P56 (Fig. 3p, q). These results indicate an age-dependent increase in ubiquitin-containing inclusion bodies in autophagy-deficient neurons. Consistent with the above immunohistochemical analysis (Fig. 3p, q), immunoblot analysis revealed increasing levels of high-molecular-mass polyubiquitinated proteins with age in the brains of *Atg7^{fllox/fllox}; nestin-Cre* mice (Fig. 4a), and an increase in their insoluble forms at later developmental stages (data not shown).

Finally, we examined whether autophagy deficiency influences proteasome functions. The chymotryptic activities of 26S and 20S proteasomes (measured using Suc-LLVY-MCA as a substrate) were comparable in extracts from both control and *Atg7^{fllox/fllox}; nestin-Cre* brains (Fig. 4b). Furthermore, the ATP-dependent degradation of ornithine decarboxylase (ODC) by 26S proteasomes was similar in control and mutant brains (Fig. 4c). Moreover, the relative amounts of several subunits of the 26S proteasome did not change in the brain irrespective of autophagy deficiency (as detected by immunoblotting, Fig. 4d). These results indicate that age-dependent accumulation of ubiquitin-positive aggregates in the autophagy-deficient brain occurs despite the apparently normal function of proteasomes.

Over the past decade, researchers working in the field of neurodegenerative diseases have made great progress in uncovering the mechanisms of these disorders by focusing on the interplay between proteolytic stress and neural cell death^{17,18}. Increasing evidence indicates that ubiquitin-positive inclusion bodies—the pathological hallmark of various neurodegenerative diseases—are formed by dysfunction of proteasome degrading machinery³. Indeed, proteins with aberrant structure impair proteasome functions directly, thus attenuating ‘garbage disposal’¹⁹. On the other hand, the accumulation of autophagosomes owing to impairment of fusion with lysosomes is observed in various disorders, including Alzheimer’s disease^{20–22}, and it has been proposed that autophagy functions to degrade toxic proteins in familial neurodegenerative diseases^{23–25}. However, it remains unknown whether these two proteolytic systems work independently or cooperatively to maintain protein homeostasis in cells. Furthermore, whether autophagy has a role in cell death or cell survival is currently under debate²⁶.

We have shown that *Atg7^{fllox/fllox}; nestin-Cre* mice exhibit neurological abnormalities and neuronal death, suggesting that impaired autophagy causes neurodegeneration. We suggest a particularly important role for autophagy in the brain, to which nutrients must be constantly supplied from other organs, even under fasting conditions. Moreover, we find that autophagy deficiency in neurons leads to the accumulation of ubiquitin-containing inclusion bodies,

without obvious deficits in proteasome function. Hence, our data indicate a central role for constitutive autophagy in the elimination of unfavourable proteins and in the survival of neurons, independent of the proteasome system (see the proposed model in Supplementary Fig. S4). Although we do not know whether autophagy and proteasome degradation target a similar set of normal and/or misfolded proteins, it is plausible that the autophagic pathway assists in degrading accumulated intractable proteins when cellular levels of aberrant proteins overwhelm the disposal capacity of the proteasome.

We have shown that a lack of autophagy is associated with neurodegeneration, even in the absence of harmful gene products found in neurodegenerative disorders such as Huntington's disease, Parkinson's disease and amyotrophic lateral sclerosis. We therefore predict that the role of autophagy becomes even more critical in the pathogenesis of such neurodegenerative diseases, when disease-related, aggregation-prone proteins are expressed as a result of genetic mutations and/or environmental insults, leading to early-onset symptoms.

METHODS

Animals. Nestin-*Cre* transgenic mice¹⁴ were purchased from the Jackson Laboratory. *Atg7^{fllox/fllox}* mice⁸ were bred with nestin-*Cre* transgenic mice to produce *Atg7^{fllox/fllox}*; nestin-*Cre* mice. Mice were housed in a pathogen-free facility. Motor function was assessed using a rotarod test²⁷. Experimental protocols were approved by the Ethics Review Committee for Animal Experimentation at the Tokyo Metropolitan Institute of Medical Science.

Immunoblot analysis. Immunoblots were carried out as described previously⁸. Antibodies against Atg7, Atg5 and LC3 have been described previously⁸. Antibodies against Rpt1, Rpn2 and $\alpha 5$ were provided by K. B. Hendil. Polyclonal anti-ubiquitin (FK2; Medical & Biological Laboratories) and anti-actin (MAB1501R; Chemicon) antibodies were also used.

Histological examination. *Atg7^{fllox/+}*; nestin-*Cre* and *Atg7^{fllox/fllox}*; nestin-*Cre* mice were fixed by cardiac perfusion with 0.1 M phosphate buffer containing 4% paraformaldehyde, 4% sucrose for light microscopy and immunohistochemistry, with 0.1 M phosphate buffer containing 2% paraformaldehyde, 2% glutaraldehyde for standard electron microscopy, or with 0.1 M phosphate buffer containing 4% paraformaldehyde, 0.1% glutaraldehyde for immunoelectron microscopy. Brain tissues were excised and processed for morphological analysis as described previously^{8,28}. For light microscopic analysis, 10- μ m cryosections were cut and stained with H&E or immunolabelled with the following antibodies: anti-human NeuN (Abcam), anti-GFAP (Sigma), anti-calbindin (Sigma), anti-myelin basic protein (MBP; MCA409S, Serotec) and anti-ubiquitin (DAKO) antibodies. The TUNEL assay has been described previously²⁸. For counting TUNEL-positive signals in the cerebral cortex, 60 coronal sections containing the anterior portion of the hippocampus (~0.6-mm thick in total) were cut, and TUNEL staining was performed on every sixth section, on a total of ten sections.

Electron microscopy and immunoelectron microscopy. Fixed brains were post-fixed with 1% OsO₄, embedded in Epon812 and sectioned. Immunoelectron microscopy was carried out on cryo thin sections as described previously²⁹. In brief, brains were frozen in phosphate buffer containing 2.3 M sucrose and 20% polyvinyl pyrrolidone. Ultrathin sections were mounted on Formvar carbon-coated nickel grids, blocked with 1% bovine serum albumin (BSA) in PBS, and incubated with anti-ubiquitin antibody (1B3) and colloidal gold-conjugated secondary antibody.

Glycerol gradient analysis. Samples were fractionated by 10–40% (v/v) linear glycerol density gradient centrifugation (22 h, 100,000g) as described previously³⁰.

Assay of proteasome activity. Peptidase activity was measured using a fluorescent peptide substrate, succinyl-Leu-Leu-Val-Tyr-7-amido-4-methylcoumarin (Suc-LLVY-MCA), as described previously³⁰. Ornithine decarboxylase (ODC)-degradation activity was assayed as described previously³⁰.

Received 6 February; accepted 20 March 2006.

Published online 19 April 2006.

1. Forman, M. S., Trojanowski, J. Q. & Lee, V. M. Neurodegenerative diseases: a decade of discoveries paves the way for therapeutic breakthroughs. *Nature Med.* **10**, 1055–1063 (2004).
2. Shintani, T. & Klionsky, D. J. Autophagy in health and disease: a double-edged sword. *Science* **306**, 990–995 (2004).
3. Goldberg, A. L. Protein degradation and protection against misfolded or damaged proteins. *Nature* **426**, 895–899 (2003).
4. Reggiori, F. & Klionsky, D. J. Autophagosomes: biogenesis from scratch? *Curr. Opin. Cell Biol.* **17**, 415–422 (2005).

5. Levine, B. & Klionsky, D. J. Development by self-digestion: molecular mechanisms and biological functions of autophagy. *Dev. Cell* **6**, 463–477 (2004).
6. Tsukada, M. & Ohsumi, Y. Isolation and characterization of autophagy-defective mutants of *Saccharomyces cerevisiae*. *FEBS Lett.* **333**, 169–174 (1993).
7. Kuma, A. *et al.* The role of autophagy during the early neonatal starvation period. *Nature* **432**, 1032–1036 (2004).
8. Komatsu, M. *et al.* Impairment of starvation-induced and constitutive autophagy in *Atg7*-deficient mice. *J. Cell Biol.* **169**, 425–434 (2005).
9. Melendez, A. *et al.* Autophagy genes are essential for dauer development and life-span extension in *C. elegans*. *Science* **301**, 1387–1391 (2003).
10. Juhasz, G., Csikos, G., Sinka, R., Erdelyi, M. & Sass, M. The *Drosophila* homolog of Atf1 is essential for autophagy and development. *FEBS Lett.* **543**, 154–158 (2003).
11. Paludan, C. *et al.* Endogenous MHC class II processing of a viral nuclear antigen after autophagy. *Science* **307**, 593–596 (2005).
12. Nakagawa, I. *et al.* Autophagy defends cells against invading group A *Streptococcus*. *Science* **306**, 1037–1040 (2004).
13. Gutierrez, M. G. *et al.* Autophagy is a defense mechanism inhibiting BCG and *Mycobacterium tuberculosis* survival in infected macrophages. *Cell* **119**, 753–766 (2004).
14. Betz, U. A., Voshchenrich, C. A., Rajewsky, K. & Muller, W. Bypass of lethality with mosaic mice generated by Cre-loxP-mediated recombination. *Curr. Biol.* **6**, 1307–1316 (1996).
15. Ohsumi, Y. Molecular dissection of autophagy: two ubiquitin-like systems. *Nature Rev. Mol. Cell Biol.* **2**, 211–216 (2001).
16. Kabeya, Y. *et al.* LC3, a mammalian homologue of yeast Apg8p, is localized in autophagosomal membranes after processing. *EMBO J.* **19**, 5720–5728 (2000).
17. Ciechanover, A. & Brundin, P. The ubiquitin proteasome system in neurodegenerative diseases: sometimes the chicken, sometimes the egg. *Neuron* **40**, 427–446 (2003).
18. Bossy-Wetzell, E., Schwarzenbacher, R. & Lipton, S. A. Molecular pathways to neurodegeneration. *Nature Med.* **10** (Suppl.), S2–S9 (2004).
19. Bence, N. F., Sampat, R. M. & Kopito, R. R. Impairment of the ubiquitin-proteasome system by protein aggregation. *Science* **292**, 1552–1555 (2001).
20. Yu, W. H. *et al.* Macroautophagy—a novel β -amyloid peptide-generating pathway activated in Alzheimer's disease. *J. Cell Biol.* **171**, 87–98 (2005).
21. Tanaka, Y. *et al.* Accumulation of autophagic vacuoles and cardiomyopathy in LAMP-2-deficient mice. *Nature* **406**, 902–906 (2000).
22. Nishino, I. *et al.* Primary LAMP-2 deficiency causes X-linked vacuolar cardiomyopathy and myopathy (Danon disease). *Nature* **406**, 906–910 (2000).
23. Webb, J. L., Ravikumar, B., Atkins, J., Skepper, J. N. & Rubinsztein, D. C. α -Synuclein is degraded by both autophagy and the proteasome. *J. Biol. Chem.* **278**, 25009–25013 (2003).
24. Ravikumar, B. *et al.* Inhibition of mTOR induces autophagy and reduces toxicity of polyglutamine expansions in fly and mouse models of Huntington disease. *Nature Genet.* **36**, 585–595 (2004).
25. Fortun, J., Dunn, W. A. Jr, Joy, S., Li, J. & Notterpek, L. Emerging role for autophagy in the removal of aggregates in Schwann cells. *J. Neurosci.* **23**, 10672–10680 (2003).
26. Levine, B. & Yuan, J. Autophagy in cell death: an innocent convict? *J. Clin. Invest.* **115**, 2679–2688 (2005).
27. Bontekoe, C. J. *et al.* Knockout mouse model for *Fxr2*: a model for mental retardation. *Hum. Mol. Genet.* **11**, 487–498 (2002).
28. Koike, M. *et al.* Involvement of two different cell death pathways in retinal atrophy of cathepsin D-deficient mice. *Mol. Cell. Neurosci.* **22**, 146–161 (2003).
29. Waguri, S. *et al.* Cysteine proteinases in GH4C1 cells, a rat pituitary tumour cell line, are secreted by the constitutive and regulated secretory pathways. *Eur. J. Cell Biol.* **67**, 308–318 (1995).
30. Tanahashi, N. *et al.* Hybrid proteasomes. Induction by interferon- γ and contribution to ATP-dependent proteolysis. *J. Biol. Chem.* **275**, 14336–14345 (2000).

Supplementary Information is linked to the online version of the paper at www.nature.com/nature.

Acknowledgements We thank T. Kaneko, T. Kouno and K. Tatsumi for technical assistance. We also thank A. Yabashi, K. Kanno, F. Kaji and K. Ikeue for help with morphological analysis, J. Ezaki for discussion, and Z. Yue for critical reading of the manuscript. This work was supported in part by a Grant-in-Aid from the Ministry of Education, Culture, Sports, Science and Technology of Japan.

Author contributions M.K. and T.C. generated *Atg7^{fllox/fllox}* mice, and M.K. and J.I. performed most of the experiments to characterize *Atg7^{fllox/fllox}*; nestin-*Cre* mice. S.W. performed histological and microscopic analyses, and S.M. performed the biochemical analysis of proteasome activity. M.K., S.W. and K.T. wrote the paper. All authors discussed the results and commented on the manuscript.

Author Information Reprints and permissions information is available at npg.nature.com/reprintsandpermissions. The authors declare no competing financial interests. Correspondence and requests for materials should be addressed to K.T. (tanakak@rinshoken.or.jp).